Quantum Information Processing, Vol. 3, Nos. 1–5, October 2004 (© 2004)

Quantum Computer Development with Single Ion Implantation

A. Persaud,[1] S. J. Park,[1] J. A. Liddle,[1] I. W. Rangelow,[2] J. Bokor,[1,3] R. Keller,[1] F. I. Allen,[1] D. H. Schneider,[4] and T. Schenkel[1]

Received February 9, 2004; accepted March 15, 2004

Spins of single donor atoms are attractive candidates for large scale quantum information processing in silicon. Formation of devices with a few qubits is crucial for validation of basic ideas and development of a scalable architecture. We describe our development of a single ion implantation technique for placement of single atoms into device structures. Collimated highly charged ion beams are aligned with a scanning probe microscope. Enhanced secondary electron emission due to high ion charge states (e.g., $^{31}P^{13+}$, or $^{126}Te^{33+}$) allows efficient detection of single ion impacts. Studies of electrical activation of low dose, low energy implants of ^{31}P in silicon show a drastic effect of dopant segregation to the SiO_2/Si interface, while Si_3N_4/Si retards ^{31}P segregation. We discuss resolution limiting factors in ion placement, and process challenges for integration of single atom arrays with control gates and single electron transistors.

KEY WORDS: Electron emission; single electron devices; Coulomb blockade; ion doping; scanning probe; quantum computation.

PACS: 03.67.Lx, 34.50.Dy, 85.35.Gv, 73.23, 61.72, 86.40.py, 07.79.−v.

1. INTRODUCTION

Several promising proposals for implementation of large scale quantum information processing devices in solids are based on the manipulation

[1]E. O. Lawrence Berkeley National Laboratory, Berkeley, CA 94720, USA. E-mail: T_Schenkel@LBL.gov
[2]Institute of Microstructure Technologies and Analytics, University of Kassel, 34109 Kassel, Germany.
[3]Department of Electrical Engineering and Computer Science, University of California, Berkeley, CA 94720, USA.
[4]Lawrence Livermore National Laboratory, Livermore, CA 94550, USA.

1570-0755/04/1000-0233/0 © 2004 Springer Science+Business Media, Inc.

of spins of electrons and nuclei of single dopant atoms.[1–3] The accurate placement of single atoms and their integration with control gates and readout structures (such as single electron transistors) represents a nanofabrication challenge that needs to be mastered in order to be able to test, validate and improve device architectures. Spins of electrons of phosphorous atoms are the most attractive candidates to date, since their decoherence time is quite long ($\sim$60 ms for isolated donors),[4] and their integration in a silicon matrix allows use of a highly developed semiconductor processing infrastructure.

In this article we describe our program on single atom array formation by single ion implantation, and the integration of single P-atom arrays with control gates and readout SETs.[5,6]

2. SINGLE ION IMPLANTATION

In single ion implantation, every ion impact has to be detected, and the position of each ion impact has to be controlled with high resolution and accuracy.[6–8] The ease or difficulty of detecting single ions depends on their energy and charge state. Low energy ($<$ 20 keV), singly charged ions are difficult to detect, because emission of secondary electrons from inelastic collisions ("kinetic electron emission") is ineffective with secondary electron yields of one or less than one electron per ion.[9] Detection in the bulk of a detector is difficult because most of the ion's energy is dissipated in elastic collisions and not in the formation of electron hole pairs. This is especially so for low energy heavy ions (e.g., Te at 20 keV), where only about 10% of the ion energy is transferred into measurable electronic excitations in the solid. Using high charge state ions allows efficient detection of single ions, because secondary electron emission is proportional to the ion charge state, $Y_e \sim 1.5 \times q$, and tens to hundreds of electrons can be emitted from single ions.[10] Secondary electron emission from high charge state ions is rather insensitive to the ions kinetic energy for ion energies above 2 keV. Secondary electron emission yields increase for very low impact energies (below 2 keV) due to increased time for above surface charge relaxation.[11]

Next to detection, the second challenge in single ion implantation is to ensure accurate alignment and high resolution in ion placement. In conventional focused ion beam systems, beams of Ga^+ ions are focused to a spot size of $\sim$ 10 nm (full width half maximum of a beam with approximately Gaussian shape). This is enabled by the high brightness of the liquid metal ion source used to form Ga^+ beams.[12] While progress is being made in source development, the brightness of highly charged ion

sources still remains orders of magnitude lower than that of liquid metal ion guns.[13] Besides beam resolution, i.e., spot size, the accuracy of alignment is crucial for placement of ions into desired positions. Alignment is complicated by the fact that the ion beam must not be used for imaging of the region of interest since this would be accompanied by undesired implantation.

A schematic of our single ion implantation setup is shown in Fig. 1. Beams of highly charged dopant ions are extracted from our electron beam ion trap/source.[14] Typical ion beam energies are 1–10 kV $\times q$, where q is the charge of the selected ion species. Specific ion species are selected by momentum analysis in a double focusing bending magnet. The beam is first focused by a series of electrostatic lenses and is then collimated by a set of apertures. Ions transmit the nanometer scale apertures at a rate of a few ions per second.[15] When a highly charged dopant ion reaches a wafer surface, the potential energy that corresponds to its high charge state is released. Once the ion reaches a critical distance above the

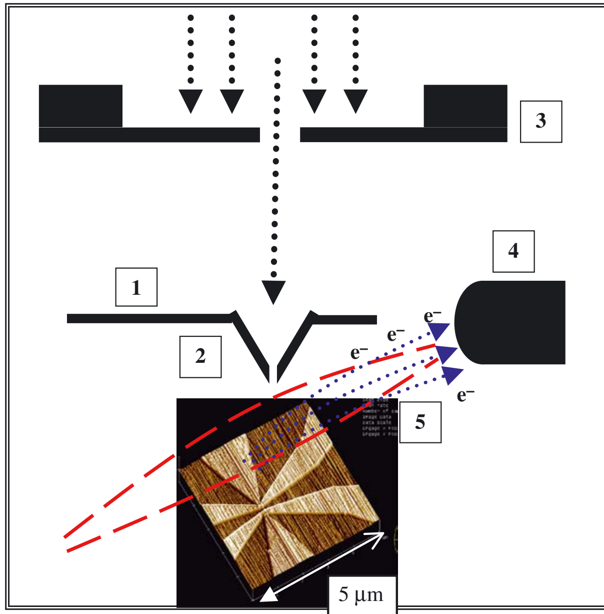

Fig. 1. Schematic illustration of the Single Ion Implantation setup with SFM alignment. Piezo-resistive cantilever with hollow tip (1) and small aperture (2), mounted on a pre-collimation membrane (3), and secondary electron detector (4). The sample is an SET pair shown here in a scanning force microscope image (5, planar view). Dashed lines indicate magnetic field lines for guidance of secondary electrons to the detector.

surface, it can capture electrons from the solid into excited Rydberg states, while vacancies in inner shells remain empty. This process, also referred to as formation of a transient "hollow atom", is very effective and the ion actually neutralizes completely before it impinges on the surface. Rapid di-electronic processes mediate the relaxation to the ground state. The ion travels only for about 10 fs in the solid during dissipation of the potential energy.(16) Secondary electron emission yields depend on the specific material. For $^{31}P^{13+}$ on silicon with a native oxide, about 20 electrons are emitted by each ion. It is important to note that these electrons are emitted within less than 100 fs. Most of the secondary electrons have energies of ~5–20 eV. The beam collimating aperture is formed in the tip of a scanning force microscope, and the tip is placed in close proximity ($< 5\,\mu m$) to the sample surface to minimize beam divergence. In order to maximize the extraction efficiency of secondary electrons into the detector, we formed a magnetic guide field with an angle of 10° with respect to the surface. Secondary electrons spiral along the magnetic field lines to the surface of a plastic scintillator. The scintillator is biased at high voltage (10–18 kV). Electrons are stopped in the scintillator and a fraction of their energy is converted into electronic excitations which relax radiatively. A typical conversion efficiency is 100 photons per 10 keV electron. Photons are emitted with a decay time of about 2 ns, and are guided through a Teflon coated quartz light guide to a photo multiplier tube (PMT). The PMT detects photons from the scintillator (central wavelength 425 nm) with a quantum efficiency of 15–20%. Multiple photons arrive as a burst and the resulting avalanche of electrons produces a pulse with a height proportional to the number of secondary electrons collected from a single ion impact. The detection of multiple secondary electrons in a burst is crucial since this allows us to discriminate spurious background in the PMT from the pulse height spectrum. Single electron or single photon background events are well separated from true single ion impact events. Examples of pulse height distributions are shown in Fig. 2 for Te^{33+} and P^{13+} ions with kinetic energies of $3\,kV \times q$. Tellurium, a double donor in silicon, is a candidate for implementation of spin dependent charge measurements.(17) Atoms of both phosphorous and tellurium were injected into the highly charged ion source by evaporation of solid stock in ovens. The detection efficiencies for single ions of P^{13+} and Te^{33+} are 85% and 95%, respectively. The collection efficiency for secondary electrons, and guidance of photons to the PMT has been optimized to achieve 100% detection efficiency for Xe^{40+}. In these measurements some background from high energy events in the scintillator was present. This background was reduced by reduction of the scintillator voltage, and allowed us to detect Xe^{32+} ions with 85% efficiency and zero background in the main peak region

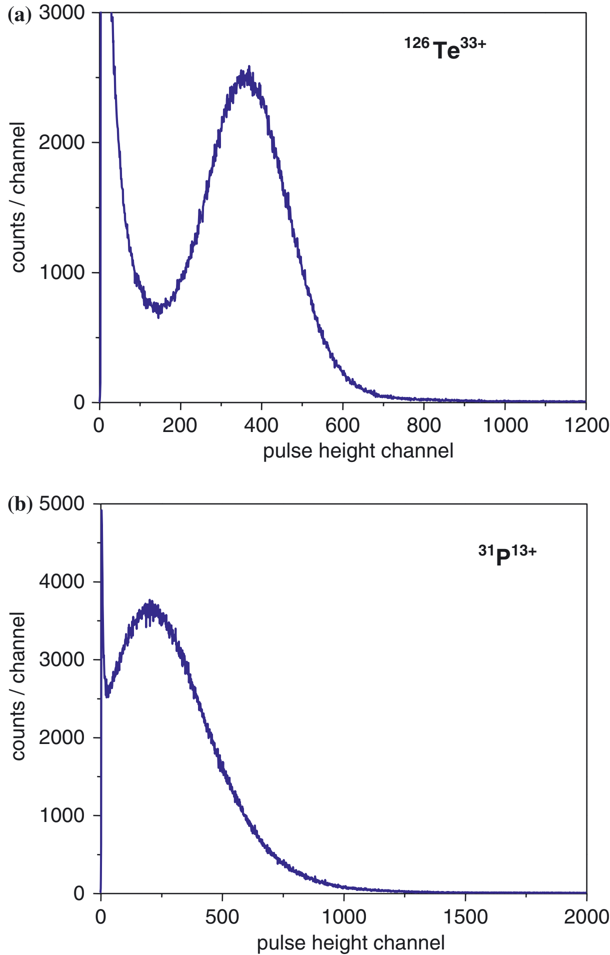

Fig. 2. Pulse height distributions from detection of secondary electrons bursts following the impact of $^{126}Te^{33+}$ (a) and $^{31}P^{13+}$ ions (b). The detection efficiencies were 95% and 85% respectively.

over periods of hours. Here, ions were not decelerated and their kinetic energies corresponded to a 5 kV extraction potential. Detection of very low energy heavy ions was achieved by deceleration at the target, and we detected 7 keV Xe^{32+} ions also with 85% efficiency.[6] With further optimization of the secondary electron collection and reduction of losses in the light pipe from the scintillator to the PMT we anticipate to be able to

detect low energy P^{13+} ions with 100% efficiency integrated with scanning probe alignment.

The aperture that defines the beam spot is formed in the tip of a scanning force microscope (SFM). The SFM is based on piezoelectric sensors with a Wheatstone bridge circuit formed in silicon cantilevers.[18] The SFM is needed to allow accurate alignment of the ion beam with marker structures on the samples. An alignment accuracy of ~5 nm is highly desirable for effective device development. The probe tip is a hollow pyramid into which a large hole (~500 nm diameter) is drilled with a FIB (Fig. 3). The SFM cantilever is mounted on a silicon nitrite membrane, and when the hole is drilled in the tip, a second hole is also pierced through the membrane. These two holes are aligned and the membrane provides additional beam collimation. The large hole in the tip is then reduced in diameter by monitored, *in situ* thin film deposition.[19] Holes with diameters as small as 4.3 nm have been formed this way. Additionally, "sensing poles", i.e., poles with radii of curvature of less than 50 nm to ensure high imaging resolution have been formed by electron beam assisted deposition of

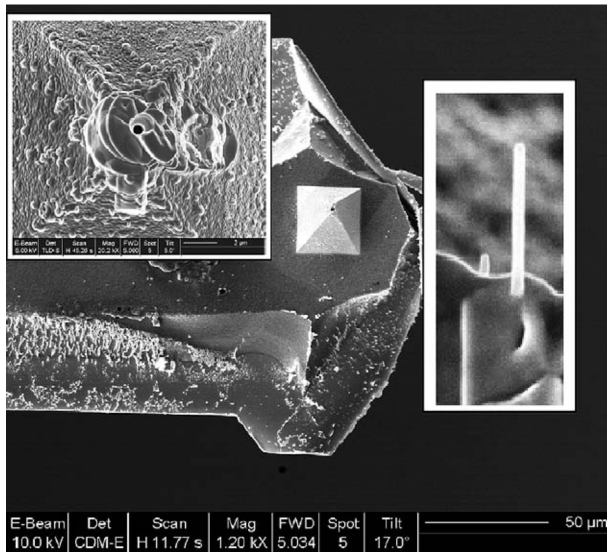

Fig. 3. SFM cantilever with hollow pyramid tip. A hole was drilled in a single step both through the tip and the membrane on which the cantilever is mounted. The hole in the membrane is visible due to the tilt angle of 17°. The insert on the top left shows a hole that went through several cycles of drilling and closing by electron beam assisted Pt deposition, and redrilling. The insert on the right shows a 90 nm wide "sensing pole" grown next to a hole with reduced diameter.

Pt. The sensors of the piezoresistive SFM allow imaging of the surface topography in conventional contact mode, and also in tapping mode with rapid thermal actuators.[20] The latter is important for increased imaging and alignment speed. To date, our SFM with sensors have been operated in vacuum and integration with the implant beam is in progress. Studies of tip lifetime and charge exchange of ions during transmission of the apertures indicate that the tips are robust for days of exposure to ion beams with nA intensities.[5]

3. ACTIVATION OF LOW DOSE, LOW ENERGY P IMPLANTS IN SILICON

Ion implantation is accompanied by damage to the host crystal as incident ions transfer energy to target atoms in elastic collisions. Atoms are displaced from their lattice positions, forming vacancies and interstitials. A fraction of these defects anneals during the collision cascade that accompanies the slowdown process of the incident ions. Implanted ions come to rest mostly on interstitial positions in the lattice. Following implantation, arrays of P atoms have to be annealed in order to incorporate the P atoms into the silicon lattice, and to heal implantation damage to the silicon crystal. Incorporation into the lattice ensures that the bound excess electrons (at low temperature) exhibit the quasi hydrogenic wave function that makes them so attractive for quantum information processing. A qubit spacing of 20 nm corresponds to $\sim 10^{11}$ P-atoms/cm^2, representing a regime of ultra low dose in ion implantation. Diffusion during activation annealing of dopants in silicon is a well studied problem, but most studies have focused on the high dose ($> 10^{13}$ cm^{-2}) regime relevant for conventional silicon devices.[21] For low energy implants with a shallow range, the interface to the silicon crystal plays a crucial role during annealing. Phosphorous diffusion is mediated by silicon interstitials. The SiO_2/Si interface injects interstitials during annealing, and this leads to the segregation of P atoms to the interface. The consequence of this segregation effect is that P atoms are not electrically active, since they are bound at the interface, and that any pre-formed atom array is completely dissolved. Even a "perfect" SiO_2/Si interface can absorb a dose of at least 10^{12} P/cm^2.[22] The Si_3N_4/Si interface shows a complementary effect, since it injects vacancies during annealing. Vacancies retard P diffusion in Si. We have studied the activation of low dose P implants in Si and use spreading resistance analysis (SRA) as a method for characterization of carrier concentrations. SRA has exquisite sensitivity (down to at least 10^{12} carriers/cm^3), but the depth resolution is limited to about 5 nm, and the accuracy of absolute carrier levels is also limited (error of

~25%). However, SRA does allow the qualification of trends, where depth profiling with secondary ion mass spectrometry (SIMS) is in turn limited by a detection efficiency for ^{31}P in Si of about $10^{16}\,cm^{-3}$. In Fig. 4, we show SRA depth profiles of carrier concentrations for silicon (100) samples (5 Ω cm, n-type), implanted with a phosphorus dose of 10^{11} P/cm^2. Samples were annealed for 10 s at 1000 °C in a dry nitrogen atmosphere. The implant energies were 15, 30 and 60 keV. We compare samples with

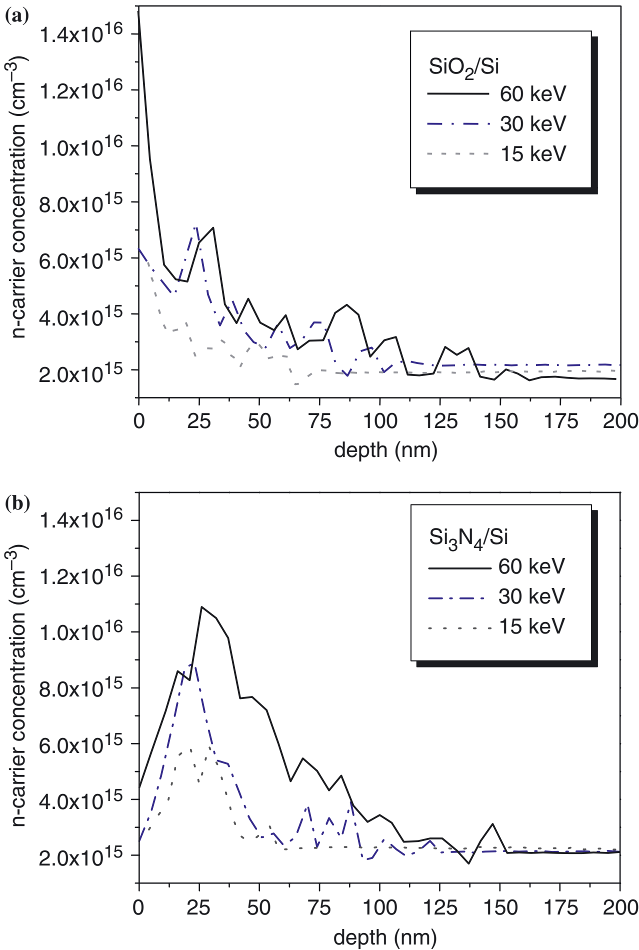

Fig. 4. SRA depth profiles of carrier concentration for silicon samples with SiO_2 (a) and Si_3N_4 (b) layers. The implant dose was 10^{11} ^{31}P/cm^2, and implant energies were 60, 30 and 15 keV.

a 5 nm thick SiO_2 layer and a 7 nm thick Si_3N_4 layer. For the oxide, a large fraction of the dose is driven to the interface, while the nitride retards dopant movement. The fraction of activated dopants increases with the implant energy from 25% to 75% for both interfaces. Residual oxygen from water in the ambient of the annealing chamber might contribute to some dopant deactivation also for the samples with silicon nitride interface. Increasing the number of available vacancies during annealing by co-implantation with Si^+ increases the activation probability,(5) and experiments are underway to combine co-implantation with Si_3N_4/Si interfaces to achieve full electrical activation of low energy, low dose implants.

This effect of enhanced dopant segregation rules out the use of SiO_2 interfaces close to P atom arrays. An additional reason to abandon SiO_2 (and Si_3N_4) is that electrical defects in amorphous dielectrics are sources of random polarization that preclude large scale spin qubit integration. We are currently developing a dielectric free, metal silicide based process for epitaxial integration of P atom arrays.

Small scale test devices are important for proof of principle demonstrations. While SiO_2 is incompatible with phosphorus, it is not with antimony. Antimony diffusion is mediated by vacancies,(21) and retarded by interstitials, making formation of Sb atom devices with SiO_2/Si interfaces an attractive test bed for single atom electronics.

4. SINGLE ELECTRON TRANSISTORS IN SILICON

Single electron transistors (SET) are sensitive electrometers that make them prime candidates for implementation of single spin measurements in spin dependent charge measurements.(17) We have formed SET pairs in SOI in order to develop two atom devices for single charge transfer experiments. An example of an SET pair is shown in Fig. 5, together with a typical $I-V$ curve of source-drain current and voltage. Coulomb blockade effects have been studied in silicon nanostructures for many years.(23) Patterning of SOI with electron beam lithography allows reliable formation of silicon nanowires down to 10 nm line width.(5,6) Mechanisms for formation of effective tunnel barriers are controversial. While deliberate tunnel barriers can be formed, charging effects also result from defects and dopant fluctuations. In our fabrication process, silicon nanowires are defined using the negative resist hydrogen silsesquioxane (HSQ) together with an organic resist in a bi-layer electron beam lithography process.(6) Nanowire size reduction by oxidation was not applied, due to direct lithographic access to features around 10–15 nm. The SET with a 14 nm wide wire had a capacitance of 10 aF and a charging energy of about 10 meV. SOI is a very attractive material for formation of single atom test devices

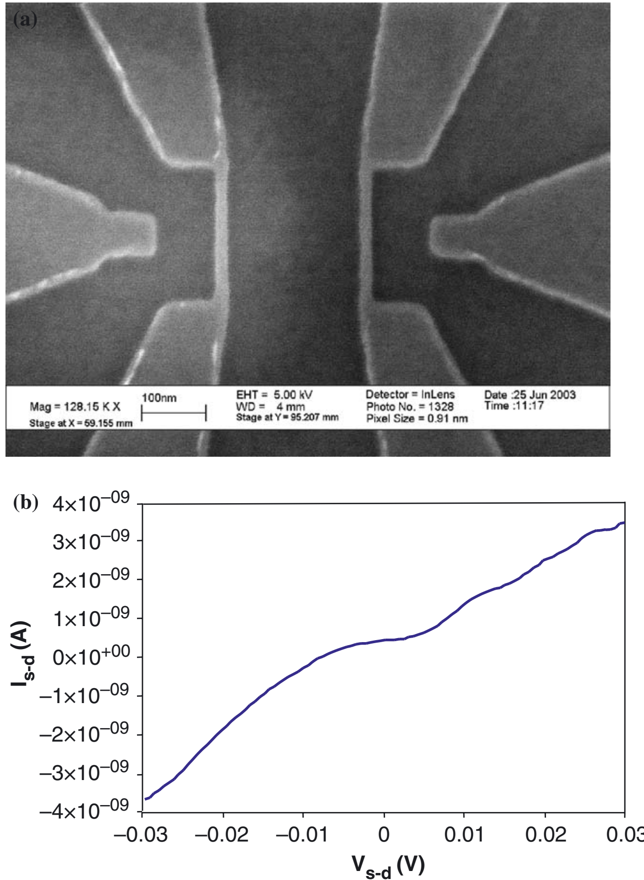

Fig. 5. Scanning electron micrograph of an SET pair in SOI (a) and typical Coulomb blockade signature in the I–V curve of a device with 14 nm wide silicon wire. The temperature was 4.2 K, and the gate voltage 20 mV.

since charging energies are large enough to allow testing at liquid helium temperatures. SET pair structures with a few Sb dopants are promising for single electron transfer tests, but large scale integration requires the development of a dielectric free architecture.

5. OUTLOOK

The effective ion placement resolution that can be achieved with single ion implantation is limited by the following contributions: (1) Range straggling from statistical energy loss processes leads to a distribution

of implantation depths. Range straggling is proportional to the implant energy, and implantation with very low energies (< 1 keV) can achieve placement accuracies of a few nm. For heavier ions, implantation into a given mean depth is accompanied by smaller range straggling. E.g., the range straggling for implantation into a depth of 20 nm is 9 nm for 13 keV P, but only 6 nm for 25 keV Sb ions. (2) The beam spot size can be controlled with the aperture size in the SFM tip, and ~5 nm wide apertures have been formed. Ion transport through nanotubes (carbon, or boron nitride based) would reduce the aperture size to 1–2 nm, and experiments are underway to test the efficiency of nanotube ion guides. (3) Alignment to markers can be achieved with scanning force microscopy to an imaging resolution of 1–5 nm. (4) Diffusion during annealing can completely dissolve atom arrays. Most dopants diffuse through distinct and specific mechanisms.[21] Phosphorous diffuses in silicon through interstitials, while antimony diffuses through vacancies. P diffusion is retarded by silicon nitride (which injects vacancies), while antimony diffusion is retarded by silicon dioxide (which injects interstitials). Choice of appropriate dopant interface combinations can reduce dopant movement during annealing to a few nm. Taking these contributions into account we conclude that an overall placement accuracy of 5–10 nm is possible with our current single ion implantation approach, and this enables the formation of prototype devices for spin qubits. A placement resolution below 5 nm will be possible if low energy ions can be transported through nanotubes efficiently. While single atom placement by scanning tunneling microscope (STM) based hydrogen lithography has atomic resolution in single atom placement, issues of diffusion and segregation are dependent on device integration and remain to be resolved also for STM based arrays.[24,25] In contrast to STM, single ion implantation does not require specific surface chemistries, so that ions can be placed into any matrix, and ions across the periodic table can be implanted. It is also perceivable to form devices where the strengths of both techniques are utilized.

Integration of several thousand qubits is necessary to realize the full potential of quantum computation. The development of tools for single atom array formation, process integration and formation of device infrastructure (control gates and SETs) has to take this goal into account at every level, while also focusing on the demonstration of basic steps in single and few qubit experiments.

ACKNOWLEDGMENTS

We thank the staff of LBNL's National Center for Electron Microscopy (NCEM) and the U. C. Berkeley Microlab for their support. This

work was supported by the National Security Agency and Advanced Research and Development Activity under Army Research Office contract number MOD707501, and by the U.S. Department of Energy under contract No. DE-AC03-76SF00098. Work at LLNL was performed under the auspices of the U.S. DOE under contract No. W-7405-ENG-48.

REFERENCES

1. B. E. Kane, *Nature* **393**, 133 (1998).
2. A. J. Skinner, M. E. Davenport, and B. E. Kane, *Phys. Rev. Lett*. **90**, 087901 (2003).
3. R. Vrijen, E. Yablonovitch, K. Wang, H. W. Jiang, A. Balandin, V. Roychowdhury, T. Mor, and D. DiVincenzo, *Phys. Rev. A* **62**, 12306 (2000).
4. A. M. Tyryshkin, S. A. Lyon, A. V. Astashkin, and A. M. Raitsimring, *Phys. Rev. B* **68**, 193207 (2003).
5. T. Schenkel, A. Persaud, S. J. Park, J. Nilsson, J. Bokor, J. A. Liddle, R. Keller, D. H. Schneider, D. W. Cheng, and D. E. Humphries, *J. Appl. Phys*. **94**, 7017 (2003).
6. S.-J. Park, A. Persaud, J. A. Liddle, J. Nilsson, J. Bokor, D. H. Schneider, I. Rangelow, and T. Schenkel, *Microelectr. Eng*. **73–74**, 695 (2004).
7. Yang Changyi, D. N. Jamieson, C. Pakes, S. Prawer, A. Dzurak, F. Stanley, P. Spizziri, L. Macks, E. Gauja, and R. G. Clark. *J. Appl. Phys*. **42**, 4124 (2003).
8. T. Shinnada, H. Koyama, C. Hinoshita, K. Imamura, and I. Ohdomari, *Jpn. J. Appl. Phys*. **41**, L287 (2002).
9. R. A. Baragiola, *Nucl. Instr. Meth. B* **78**, 223 (1993).
10. T. Schenkel, A. V. Barnes, M. A. Briere, A. Hamza, A. Schach von Wittenau, and D. Schneider, *Nucl. Instr. Meth. B* **125**, 153 (1997).
11. F. Aumayr, H. Kurz, D. Schneider, M. A. Briere, J. W. McDonald, C. E. Cunningham, and H. P. Winter, *Phys. Rev. Lett* **71**, 1943 (1993).
12. J. Orloff, M. Utlaut, and L. Swenson, *High Resolution Focused Ion Beams: FIB and its Applications* (Kluwer, New York, 2003).
13. R. E. Marrs, *Nucl. Instr. Meth. B* **149**, 182 (1999).
14. T. Schenkel, A. Persaud, A. Kraemer, J. W. McDonald, J. P. Holder, A. V. Hamza, and D. H. Schneider, *Rev. Sci. Instr*. **73**, 663 (2002).
15. T. Schenkel, A. Persaud, S. J. Park, J. Meijer, J. R. Kingsley, J. W. McDonald, J. P. Holder, J. Bokor, and D. H. Schneider, *J. Vac. Sci. Technol. B* **20**, 2819 (2002).
16. M. Hattass, T. Schenkel, A. V. Hamza, A. V. Barnes, M. W. Newman, J. W. McDonald, T. R. Niedermayr, G. A. Machicoane, and D. H. Schneider, *Phys. Rev. Lett*. **82**, 4795 (1999).
17. B. E. Kane, N. S. McAlpine, A. S. Dzurak, and R. G. Clark, G. J. Milburn, He Bi Sun, and Howard Wiseman, *Phys. Rev. B* **61**, 2961 (2000).
18. I. W. Rangelow, F. Shi, P. Hudek, T. Gotszalk, P. B. Grabiec, and P. Dumania, *SPIE* **2879**, 56 (1996).
19. T. Schenkel, V. Radmilovic, E. A. Stach, S.-J. Park, and A. Persaud, *J. Vac. Sci. Technol. B* **21**, 2720 (2003).
20. R. Pedrak, Tzv. Ivanov, K. Ivanova, T. Gotszalk, N. Abedinov, and I. W. Rangelow, K. Edinger, E. Tomerov, T. Schenkel, and P. Hudek, *J. Vac. Sci. Technol. B* **21**, 3102 (2003).
21. A. Ural, P. B. Griffin, and J. D. Plummer, *J. Appl. Phys*. **85**, 6440 (1999).
22. J. Dabrowski, H.-J. Müssig, V. Zavodinsky, R. Baierle, and M. J. Caldas, *Phys. Rev. B* **65**, 245305 (2002).

23. See e.g., H. Ahmed, *J. Vac. Sci. Technol. B* **15**, 2101 (1997).
24. T.-C. Shen, C. Wang, G. C. Abeln, J. R. Tucker, J. W. Lyding, Ph. Avouris, and R. E. Walkup, *Science* **268**, 1590 (1995); T.-C. Shen, J.-Y. Ji, M. A. Zudov, R.-R. Du, J. S. Kline, and J. R. Tucker, *Appl. Phys. Lett*. **80**, 1580 (2002).
25. S. R. Schofield, N. J. Curson, M. Y. Simmons, F. J. Rue®, T. Hallam, L. Overbeck, and R. G. Clark, *Phys. Rev. Lett*. **91**, 13104 (2003).